Alpha-particle spectroscopic strengths using the (p,pα) reaction at 101.5 MeV

T. A. Carey,* P. G. Roos, N. S. Chant, A. Nadasen,† and H. L. Chen‡
Department of Physics and Astronomy, University of Maryland, College Park, Maryland 20742
(Received 29 November 1983)

Proton-alpha particle coincidence spectra from 101.5 MeV (p,pα) reactions on ^{16}O, ^{20}Ne, ^{24}Mg, ^{28}Si, ^{32}S, ^{40}Ca, ^{48}Ti, ^{54}Fe, and ^{66}Zn have been obtained in a coplanar geometry at quasifree angle pairs for each target. A missing energy resolution of $\lesssim$450 keV was sufficient to separate the low-lying states of the residual nuclides. Data for ground-state transitions, and for eight excited states were obtained and compared with distorted-wave impulse approximation calculations. The target-mass dependence of the resultant relative ground-state spectroscopic factors is reasonably consistent with that obtained from (^{6}Li,d) reactions. The corresponding absolute spectroscopic factors are larger than shell-model predictions, but sensitive to the bound-state parametrization. However, the spectral shapes do constrain the range of possible bound-state rms radii. The fits to the excited states are less satisfactory.

I. INTRODUCTION

The question of the existence of multinucleon clusters as significant components of wave functions of heavier nuclei has long been a topic of investigation in nuclear physics. For example, the alpha particle model of the nucleus was first introduced in 1928 by Gamow[1] in order to explain the results of alpha-decay studies.

Experimental evidence for the existence of clusters in nuclei came forth in nuclear emulsion studies in the 1950's when protons with energies from $\simeq$40−600 MeV incident on light through heavy targets led to energy and angular distributions of emitted alpha particles which differed significantly from those expected from the statistical theory of nuclear disintegration. This overabundance of emitted alphas was consistently found to be especially large in the forward direction, thus implying direct quasifree collisions between incident protons and alpha clusters in the target nuclei. Since shell model wave functions typically have significant overlap with cluster configurations, attempts to establish additional specific clustering in nuclei require absolute comparisons of theory and experiment.

Transfer reactions have long been used as a tool of nuclear spectroscopy because of the relative simplicity of the experiments and the general success of the distorted-wave Born approximation (DWBA) in describing such reactions. Therefore, a feasible method of studying clustering in nuclei would be by performing "direct cluster transfer" reactions. Considering the alpha-pickup reaction $A(a,b)B$ (where $A=B+\alpha$ and $b=a+\alpha$) with the assumption that the four-nucleon group exists strictly as a free alpha in its ground state throughout the transfer process, the cross section in the DWBA can be written as

$$\left.\frac{d\sigma}{d\Omega}(\theta)\right|_{A(a,b)B} = S_\alpha^{AB} S_\alpha^{ab} \frac{d\sigma}{d\Omega_{\mathrm{DWBA}}}(\theta) . \quad (1)$$

Here S_α^{AB} is the alpha spectroscopic factor for the overlap of the target nucleus A with the residual nucleus B and an alpha particle, S_α^{ab}, is the alpha spectroscopic factor for the overlap of the incoming projectile a and an alpha particle with the emergent particle b, and $d\sigma/d\Omega_{\mathrm{DWBA}}$ is a DWBA cross section for the transition to a particular state of the residual nucleus which is calculated as much as for single nucleon transfer.[2–4] Thus, provided that S_α^{ab} is known, we can determine experimental values of S_α^{AB}.

Many groups have adopted this approach to the study of alpha clustering using transfer reactions; e.g., Becchetti *et al.*[5] have employed the (d,^{6}Li) reaction and Anantaraman *et al.*,[6] (^{6}Li,d), whereas Steele *et al.*[7] and Audi *et al.*[8] have used the (^{3}He,^{7}Be) reaction. Reports on further studies can be found in the conference proceedings cited in Refs. 9 and 10. On the whole these studies span the $1p$, $2s\,1d$, and $1f\,2p$ shells and in some instances extend to the region of rare-earth nuclei. Of particular interest is the extensive investigation of systematics performed by Anantaraman *et al.*[6] Figure 1 shows a graph of their extracted relative alpha spectroscopic factors for the observed

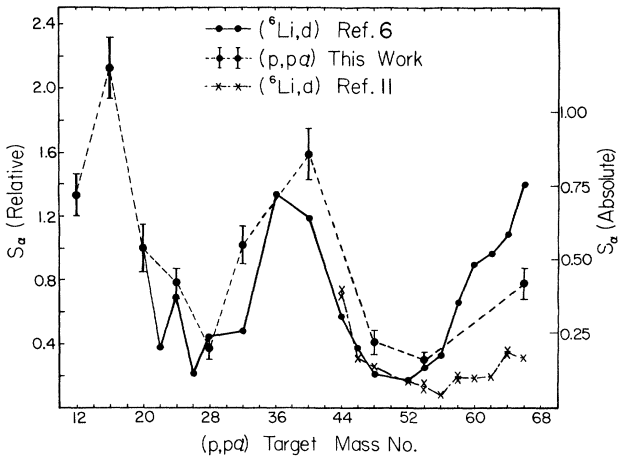

FIG. 1. Relative ground state alpha spectroscopic factors plotted as a function of the residual nucleus [target nucleus for (p,pα)]. The solid line represents the (^{6}Li,d) results of Ref. 6, and the dotted-dashed line represents a reanalysis (Ref. 11) of the same data. The dashed line is from the present analysis of (p,pα).

ground state to ground state transitions plotted as a function of the residual nucleus [target nucleus for (p,pα)] mass number. Because the uncertainties in these points due to errors in the absolute cross section measurements are less than $\sim 30\%$, it is claimed that the rather striking oscillatory behavior exhibited by the alpha strengths is significant. Neither the SU(3) model nor full $2s\,1d$ shell model calculations can account for this trend beyond $A_f = 30$. However, a number of possible drawbacks to the transfer reaction approach should be recognized:

(i) Although reactions such as (^{6}Li,d) tend to be surface localized (due to the strong absorption of ^{6}Li in nuclei), they also suffer from considerable momentum mismatch. Thus, distortion effects will tend to be important and complicated, and exact finite range computations may be essential to the analyses.

(ii) In any DWBA calculation there is a need for accurate scattering wave functions in the calculation of transfer cross sections. This implies that one must pay particular attention to the accuracy of the optical-model parameters used and especially to their consistency when studying systematics over a wide range of nuclei. The importance of this is illustrated by the work of Fulbright *et al.*,[11] who have reanalyzed the (^{6}Li,d) data on $1f\,2p$ shell nuclei from Ref. 6. They found that essentially due only to changes in the optical potentials a considerably different trend for the ground state alpha spectroscopic factors is deduced; the effect is illustrated in Fig. 1. Anantaraman, Fulbright, and Stwertka[12] carried out further analysis of the data using a ^{6}Li distorting potential radius $r_0(A^{1/3}+1.9)$ and a bound state radius $r_0(A^{1/3}+1.0)$. This reduces the spectroscopic factors for the heavier nuclei even more. Similarly, the (^{3}He,^{7}Be) analyses are greatly hampered by a general lack of knowledge of the ^{7}Be optical potential.

(iii) Perhaps least serious, but nonetheless a limitation, is the fact that the overall normalizations and therefore the absolute values of the measured strengths depend strongly on one's knowledge of the overlap $\langle b \mid [a \otimes \alpha] \rangle$ and the interaction $v_{a\text{-}\alpha}$ for the light projectile nuclei involved in the reaction. Thus, the extraction of absolute alpha spectroscopic factors from, e.g., (^{6}Li,d) experiments requires accurate information on the d-α component of the ground state structure of ^{6}Li as well as of the d-α interaction. Because of this difficulty, reliable, absolute alpha spectroscopic factors are currently unavailable from studies of alpha transfer reactions.

To overcome some of the shortcomings associated with transfer reactions as well as to complement the available transfer results, it seems appropriate to avoid binding the cluster under investigation to the projectile or the detected particle. This leads us to the use of quasifree knockout reactions to obtain information about the possible cluster structure of nuclei. Treated as a direct knockout process this reaction clearly contains the identical nuclear structure information to that in transfer reactions.

In spite of the increased difficulty with the experiment, due to the detection of two outgoing particles, the advantages derived outweigh the associated experimental difficulties. Besides the obvious advantage of not having to bind the cluster to the projectile, the flexibility of the three-body final state kinematics allows exact momentum matching irrespective of the bombarding energy. Therefore, we chose to study alpha clustering in $2s\,1d$ and $1f\,2p$ shell nuclei with (p,pα) knockout reactions. In order to reduce the effects of distortion and to be able to separate sequential decay processes from direct quasifree knockout reactions, we used the highest energy protons available from the University of Maryland Sectored Isochronous Cyclotron, namely 100 MeV protons.

The specific targets used—^{16}O, ^{20}Ne, ^{24}Mg, ^{28}Si, ^{32}S, ^{40}Ca, ^{48}Ti, ^{54}Fe, and ^{66}Zn—were predominantly $4n$-type even-even nuclei with masses chosen to sample the major features of the trend observed in the alpha transfer studies of Anantaraman *et al.*[6] A preliminary report of this work for the ground state transitions has already been published,[13] and generally confirms the oscillatory features shown in the (^{6}Li,d) reaction. In this paper we present the experimental results and the theoretical analysis in considerably more detail. In addition, we explore an alternative analysis for the bound alpha-cluster wave function using a folding model, as well as discuss the results for excited state transitions. In Sec. II we describe details of the experiment and in Sec. III we present the experimental results. DWIA analyses and deduced spectroscopic factors are discussed in Sec. IV. In Sec. V we provide a summary of the results and the conclusions derived.

II. EXPERIMENT

The experiment was performed using a 101.5 MeV proton beam from the University of Maryland Sectored Isochronous Cyclotron. In order to reduce beam-related background, the beam was sent through two 90° bending magnets and a 22° deflecting magnet to the center of a 1.5 m diameter scattering chamber. This provided a beam energy resolution $\Delta E/E \approx 0.04\%$ and an angular divergence of $\leq \pm 0.5°$. The size of the beam spot on target was 2 mm $\times$ 1.5 mm.

Isotopically pure ($\geq 96\%$), self-supporting targets were used for the ^{24}Mg, ^{48}Ti, ^{54}Fe, and ^{66}Zn runs. The Ca target was obtained by evaporating natural calcium metal. For silicon, a SiO_2 target was used. Gas targets were used for ^{16}O, ^{20}Ne, and ^{32}S. They were constituted of pure ^{16}O, ^{20}Ne, and H_2S gases at ~ 1 atm pressure in a 12.5 cm diameter gas cell with 7.6 μm Havar windows. Target thicknesses ranged from 0.5 to 2.0 mg/cm^2.

The proton detector telescope consisted of a 550 μm thick silicon ΔE detector followed by a 15 mm Ortec *G*-series HpGe *E* detector. A 220 μm silicon ΔE and a 5 mm Si(Li) *E* detector were used for the alpha arm. This system allowed the detection of $\sim 8-75$ MeV protons and $\sim 20-125$ MeV alphas. For the solid targets, circular slits subtending solid angles $\Delta\Omega_p \simeq 4.2$ msr and $\Delta\Omega_\alpha \simeq 1.3$ msr were used. Double collimating slits, subtending solid angles of $\Delta\Omega_p = 4.14$ and $\Delta\Omega_\alpha = 1.05$ msr, were employed for the gas target runs. The overall binding energy resolution for (p,pα) in all cases was better than 500 keV.

Outputs of all detectors were fed to charge sensitive preamplifiers. The linear signals from the preamplifiers provided the slow ΔE-E coincidences. For the coincidence between the two arms, the fast signals from the

ΔE preamplifiers were used as start and stop signals for a time-to-amplitude converter (TAC) in order to store both real and random events. The overall timing resolution between the two arms was $\lesssim 3$ nsec.

The four linear energy signals and the TAC signal suitably gated by all coincidence requirements were fed to 4096 channel analog-to-digital converters interfaced to an IBM 360/44 computer. One- and two-dimensional arrays of the data were created. Energy addition, particle identification, and subtraction of background resulting from random events were done by software.

The dead time of the processing electronics was measured with the aid of a four-channel pulser system, triggered at a rate proportional to the beam current. These pulses were fed to inputs at the preamplifiers and processed together with the real signals.

Since both proton and alpha data had to be obtained over a wide energy range, all the detectors were carefully calibrated over their dynamic energy range using ^{241}Am and ^{228}Th sources and p + d elastic scattering coincidences. The zero offset in the α-arm readout and the separation angle error between the two arms were also determined with p + d elastic scattering.

Each data run usually required about 200–500 μC of beam charge on target. While the data were processed on line, they were also written event by event on magnetic tape for later, more careful replay. On-line monitoring provided control over dead time, pileup, accidental rate,

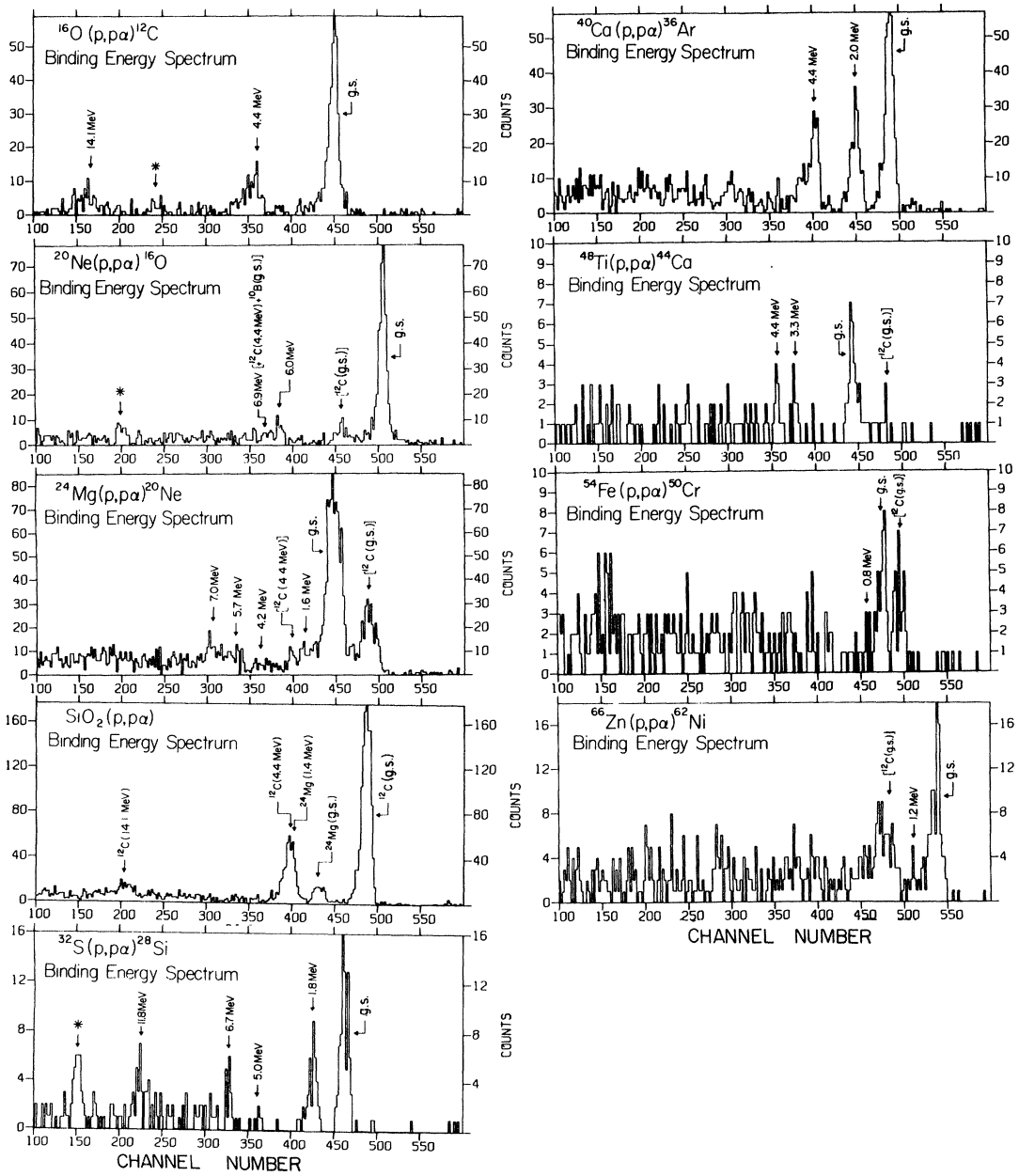

FIG. 2. Binding energy spectra obtained for the (p,pα) reaction at 100 MeV. The energies of the various states populated are indicated.

gain shifts, detector deterioration, and beam changes.

The use of essentially an identical setup for all data and careful determination of target thickness and slit geometries allows us to assign an error in the absolute cross section of about 10% and in the relative cross sections of about 6%. Thus, in general, due to the small cross sections and thereby the low yields, the relative errors between the various targets are dominated by counting statistics.

III. EXPERIMENTAL RESULTS

For all targets the (p,pα) reaction yields leading to the ground and low-lying excited states of the residual nuclei were measured. A single outgoing proton angle $\theta_p = -70.0°$ was employed, while the outgoing alpha angle was adjusted to allow zero recoil momentum for the ground state residual nucleus for each target. This geometry emphasizes the ground state $L=0$ transitions.

The binding energy spectrum for the reaction A(p,pα)B on a given target is obtained by binning the events as a function of $F3$, where $F3 = T_p + T_\alpha + T_B$, with T_p and T_α representing the kinetic energy of detected protons and alpha particles and T_B is the computed recoil energy of the residual nucleus. Figure 2 shows the binding-energy spectra for all targets. The binding-energy resolution for all targets except ^{24}Mg was less than 500 keV (FWHM), the width being dominated by target thickness effects. As expected from the experimental geometry, each spectrum contains a prominent peak corresponding to the ground state of the residual nucleus. In addition, population of some low-lying excited states is observed. Most of the excited states labeled in Fig. 2 could be clearly resolved and cross section data extracted.

Plots of the extracted energy sharing cross sections for transitions to the ground states of the residual nuclei are shown in Fig. 3. The error bars are primarily due to statistical uncertainties, since errors from other sources were small in comparison. For each spectrum the point where p_B, the residual-nucleus recoil momentum, is zero is indicated by an arrow. Each spectrum is dominated by a smooth, broad structure with a maximum close to where $\vec{p}_B = 0$, characteristic of direct $L=0$ knockout at a quasi-free angle pair.

In the region of the proton energies between 65–70

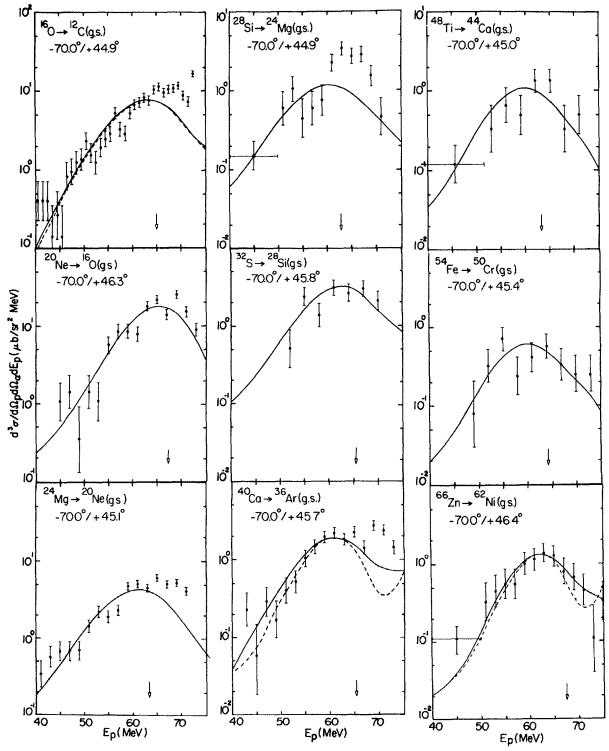

FIG. 3. Triple differential cross sections for the ground state (p,pα) reaction at 100 MeV. The solid lines represent DWIA calculations using a WS bound state geometry. Also shown for three targets are folding model calculations (dashed line).

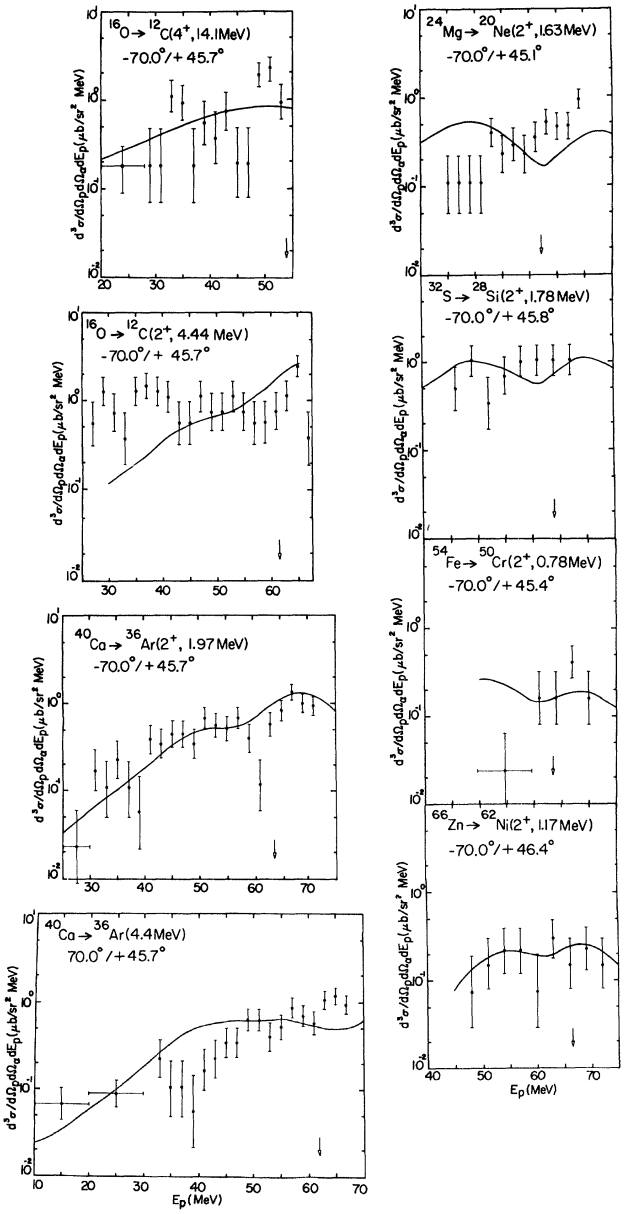

FIG. 4. Triple differential cross sections for the 100 MeV (p,pα) reaction leading to excited states of the residual nuclei. The solid lines are DWIA predictions.

MeV, many of the spectra also contain contributions from competing processes which interfere with identification of the expected quasifree peaks; most notable in this respect are the data for the ^{16}O, ^{24}Mg, ^{28}Si, and ^{40}Ca targets. We expect contributions in this region from sequential processes in which the proton inelastically scatters to a state in the target nucleus of high excitation energy which subsequently decays by alpha emission.

While the primary goal of our experiment was to obtain systematics on the ground state transitions we were also able to extract energy sharing distributions for eight $L>0$ (p,pα) transitions; these are displayed in Fig. 4. These data generally suffer from large statistical uncertainties which in turn obscure any detailed characteristics of the distributions. In fact, only in the case of

$$^{40}Ca(p,p\alpha)^{36}Ar[2^+(1.97\ MeV)]$$

can we see the distinct minimum near zero recoil momentum that is expected for direct, $L>0$ quasifree knockout; one might argue that such minima are also less obviously evident in the

$$^{16}O(p,p\alpha)^{12}C[2^+(4.44\ MeV)]$$

and

$$^{66}Zn(p,p\alpha)^{62}Ni[2^+(1.17\ MeV)]$$

distributions as well. For the most part, then, these spectra provide only loose bounds on the associated cross sections and some rather lenient tests of DWIA predictions.

An overview of the experimental results for the ground state transitions is provided by Fig. 5, which shows the peak differential quasifree (p,pα) cross sections plotted as a function of target mass number A_T. For comparison other (p,pα) measurements obtained with experimental geometries close to that employed for this experiment have also been included.[14–16] Except for the points detailed in Refs. 14 and 16 the error bars basically result from the extraction of quasifree peaks in the presence of competing processes and the statistical uncertainties.

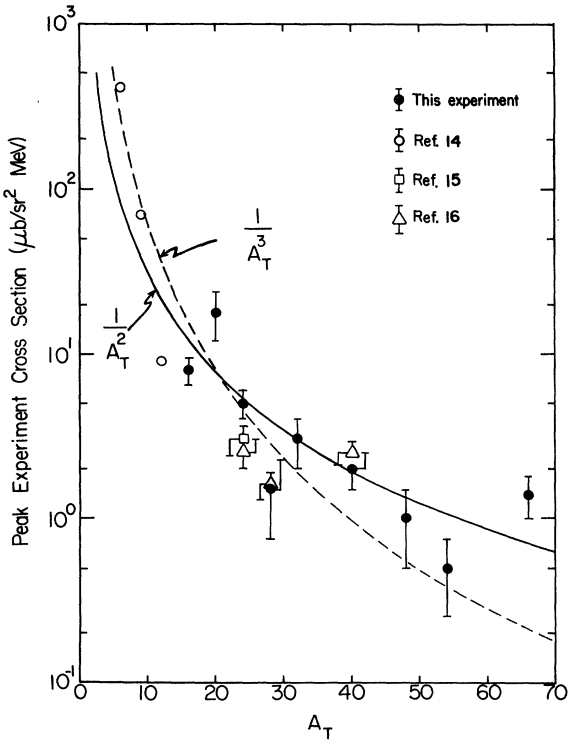

FIG. 5. Peak differential cross sections plotted as a function of target mass. The solid line depicts a $1/A_T^2$ dependence, while the dashed line represents a $1/A_T^3$ dependence.

We see that the general trend of the cross sections is a rather smooth decrease with target mass, roughly as $1/A_T^2$. Our data show local fluctuations from this behavior at $A_T=20$, 28, 54, and 66, but much of this is a manifestation of the relative target ground state Q values. It is interesting that overall this trend is quite similar to those observed for the (d,^{6}Li) (Ref. 5) and (^{3}He, ^{7}Be) (Ref. 7) peak cross sections.

IV. ANALYSIS

A. DWIA formalism

The data were analyzed in terms of the distorted wave impulse approximation (DWIA). Following Ref. 17 one can express the triple differential cross section for the knockout of an alpha particle with orbital angular moment L as

$$\frac{d^3\sigma^L}{d\Omega_p d\Omega_\alpha dT_p}=F_k S_L^\alpha \frac{d\sigma}{d\Omega}\bigg|_{p\text{-}\alpha}\sum_\lambda |T_{BA}^{\alpha L\lambda}|^2 . \quad (2)$$

F_k is a known kinematic factor, S_L^α is the alpha-spectroscopic factor for a specific final state, and $(d\sigma/d\Omega)|_{p\text{-}\alpha}$ is the two-body p-α cross section. The quantity $T_{BA}^{\alpha L\lambda}$ may be written as

$$T_{BA}^{\alpha L\lambda}=(2L+1)^{-1/2}\int \chi_p^{(-)*}(\vec{r})\chi_\alpha^{(-)*}(\vec{r}) \times\chi_p^{(+)}(\gamma\vec{r})\phi_{L\lambda}^\alpha(\vec{r})d\vec{r} , \quad (3)$$

where $\gamma=B/A$, the ratio of the residual nucleus to target mass numbers. The χ's represent the distorted waves for the incoming and outgoing particles and $\phi_{L\lambda}^\alpha$ is the bound-state wave function of the alpha cluster in the target nucleus. The quantity $T_{BA}^{\alpha L\lambda}$ is normally referred to as the distorted momentum distribution since in the limit of no distortion $T_{BA}^{\alpha L\lambda}$ is proportional to $\phi_{L\lambda}^\alpha(\vec{q})$, the Fourier transform of the alpha-cluster wave function.

It must be noted that Eq. (2) represents a factorized form of the DWIA where the two-body cross section appears as a multiplicative factor rather than a p-α t matrix within the integrand of Eq. (3). Thus $(d\sigma/d\Omega|_{p\text{-}\alpha}$ is a half-off-energy-shell cross section. In our calculations this has been replaced by an on-shell two-body cross section for the initial state or final state scattering. It has been verified[14] that the errors introduced by this on-shell approximation are quite small for moderate binding energies and that it is generally more accurate to use the cross section at the final relative energy of the p+α system.

The principal quantum number N for the bound cluster wave function was chosen on the basis of conservation of harmonic oscillator shell model quanta in the transforma-

tion from independent-particle to cluster-model wave functions. Thus, for a given L of the cluster wave function

$$2(N-1)+L=\sum_{i=1}^{4}[2(n_i-1)+l_i]\ ,$$

where n_i and l_i coincide with the filling of independent-particle shell model orbitals above the residual core.

The calculations were performed with the computer code THREEDEE written by Chant, which evaluates $T_{BA}^{aL\lambda}$ directly as a three-dimensional integral in r, θ, and ϕ using Gauss-Legendre quadrature. This method results in a tremendous saving in time in comparison to conventional angular and radial integrations via angular-momentum algebra, and produces identical results.

B. Two-body p-α cross section

One of the requirements of the calculations is a knowledge of the two-body p-α elastic scattering cross sections. For the targets used, data were needed for a range of laboratory energies $E_p=70-100$ MeV and angles $\theta_{c.m.}=85°-87°$. However, data at these exact energies and angles are not available. Therefore, interpolations of measured differential cross sections were carried out.

The data for the interpolations were obtained at proton laboratory energies of 31.0,[18] 39.8,[19] 48.8,[20] 55.0,[21] 85.0,[22] 100,[23] and 147.0 MeV.[24] Tabulated angular distributions were available for all except the 55.0 MeV data, which were extracted from a published graph. Each of these angular distributions was first smoothed by fitting it with a sum of Legendre polynomials having up to 20 terms. The differential cross section at any given energy $\tilde{E}_p$ and angle $\tilde{\theta}_{c.m.}$ was then obtained using a least squares fit of a fourth-order polynomial in $(1/E_p)$ to interpolate the computed cross sections at the angle $\tilde{\theta}_{c.m.}$ to the energy $E_p=\tilde{E}_p$.

Based on comparisons between the fits and the actual

TABLE I. Optical-model potential parameters. Note the following: All entrance channel (p + A) potential depths have been scaled by m_B/m_A.

Target (A)	Sub-channel	Particle laboratory energy (MeV)	V_0 (MeV)	r_0 (fm)	a_0 (fm)	W_0 (MeV)	r_0' (fm)	a_0' (fm)	r_{0_c} (fm)
	p + ^{16}O	101.5	19.70	1.21	0.77	5.55	1.59	0.451	1.25
^{16}O	p′ + ^{12}C	65.0	32.65	1.21	0.77	7.4	1.66	0.442	1.25
(gas and SiO_2)	α + ^{12}C	29.3	130.78	1.26	0.753	15.59	1.85	0.488	1.30
	p + ^{20}Ne	101.5	21.01	1.21	0.77	5.92	1.54	0.458	1.25
^{20}Ne	p′ + ^{16}O	67.5	32.11	1.21	0.77	7.4	1.59	0.451	1.25
	α + ^{16}O	29.3	135.71	1.26	0.760	14.81	1.81	0.489	1.30
	p + ^{24}Mg	101.5	21.89	1.21	0.77	6.17	1.52	0.464	1.25
^{24}Mg	p′ + ^{20}Ne	63.0	33.10	1.21	0.77	7.4	1.54	0.458	1.25
	α + ^{20}Ne	29.2	139.85	1.26	0.764	14.42	1.78	0.492	1.30
	p + ^{28}Si	101.5	22.51	1.21	0.77	6.34	1.50	0.469	1.25
^{28}Si	p′ + ^{24}Mg	62.5	33.21	1.21	0.77	7.4	1.52	0.464	1.25
	α + ^{24}Mg	29.0	143.45	1.26	0.766	14.19	1.75	0.497	1.30
	p + ^{32}S	101.5	22.98	1.21	0.77	6.48	1.48	0.474	1.25
^{32}S	p′ + ^{28}Si	65.6	32.54	1.21	0.77	7.4	1.50	0.469	1.25
	α + ^{28}Si	29.1	146.42	1.26	0.767	14.13	1.73	0.504	1.30
	p + ^{40}Ca	101.5	23.64	1.21	0.77	6.66	1.46	0.483	1.25
^{40}Ca	p′ + ^{36}Ar	65.0	32.65	1.21	0.77	7.4	1.47	0.479	1.25
	α + ^{36}Ar	29.5	151.01	1.26	0.767	14.24	1.69	0.519	1.30
	p + ^{48}Ti	101.5	25.98	1.21	0.77	6.78	1.44	0.491	1.25
^{48}Ti	p′ + ^{44}Ca	63.0	35.37	1.21	0.77	7.4	1.45	0.487	1.25
	α + ^{44}Ca	29.1	155.36	1.26	0.764	14.27	1.66	0.537	1.30
	p + ^{54}Fe	101.5	25.17	1.21	0.77	6.85	1.44	0.496	1.25
^{54}Fe	p′ + ^{50}Cr	64.0	33.87	1.21	0.77	7.4	1.44	0.493	1.25
	α + ^{50}Cr	29.1	157.87	1.26	0.761	14.41	1.64	0.551	1.30
	p + ^{66}Zn	101.5	26.80	1.21	0.77	6.95	1.42	0.505	1.25
^{66}Zn	p′ + ^{62}Ni	67.5	34.53	1.21	0.77	7.4	1.43	0.502	1.25
	α + ^{62}Ni	29.4	161.77	1.26	0.752	14.80	1.61	0.580	1.30

data we estimate the error in the interpolation procedure to be $\leq 10\%$ in the range of interest. Although a range of p-α cross sections are needed for the full range of the calculations, our choice of fixed proton angle greatly reduced the variation in the p-α cross section for low recoil momenta, the point of normalization of the DWIA calculations. Near $p_B=0$ the p-α cross section varied by only $\pm 3\%$ over the full range of targets. As a result any errors in relative spectroscopic factors resulting from the neglect of off-energy-shell effects should be negligible compared to the statistical errors.

C. Optical model potentials

In studying systematics over a wide range of nuclei, it is important that a consistent set of distorting optical potentials be used. For the protons, the optical model parameters were obtained from the energy- and target-mass-dependent analysis of Nadasen *et al.*[25] No spin-orbit potential was included in the DWIA calculations. The alpha potentials were derived by a systematic energy and mass interpolation of the parameters for ^{12}C, ^{24}Mg, ^{28}Si, ^{40}Ca, ^{58}Ni, and ^{90}Zr of Goldberg *et al.*,[26] the compilation of Perey and Perey,[27] and Put and Paans.[28] The interpolation was based on volume integrals and rms radii of both the real and imaginary potentials which are generally well determined in elastic scattering. To overcome the problem of discrete ambiguities inherent in low energy alpha potentials, the higher energy data ($E_\alpha > 100$ MeV) were used as a guide to obtain a unique potential family. The optical model parameters employed are listed in Table I.

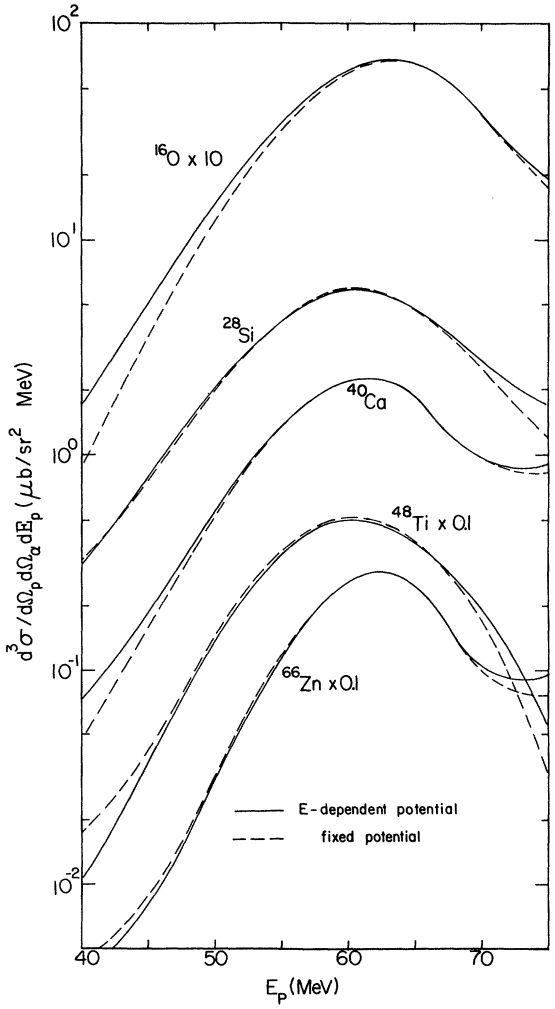

FIG. 6. DWIA calculations using (i) full energy dependent potentials over the energy sharing distribution (solid curves), and (ii) the fixed potentials listed in Table I over the entire energy sharing distribution.

The sensitivities of the calculated ground state (p,pα) energy sharing distributions to various aspects of the distorting potentials have been extensively investigated. First to be considered in this respect was the fact that the energies of the outgoing particles vary continuously over an energy sharing distribution. An investigation of the effect of the energy dependence of the optical model parameters over the energy sharing distribution was carried out for ^{16}O, ^{28}Si, ^{40}Ca, ^{48}Ti, and ^{66}Zn targets. The results are shown in Fig. 6. The solid curves represent calculations with the fully energy dependent potentials and the dashed curves were obtained by using a set of parameters evaluated at a constant energy (close to the midpoint of each distribution). The half widths at half maximum differ by $< 10\%$. Such effects are clearly negligible with regard to the extraction of spectroscopic factors. Therefore, all calculations were carried out using the constant potential parameters (see Table I) for each energy sharing distribution.

Rather large changes in the treatment of the target mass dependence of the optical potentials have relatively modest effect. For example, the potential parameters for ^{16}O and ^{40}Ca, as well as ^{40}Ca and ^{66}Zr targets were interchanged. The resulting energy sharing distributions were virtually identical in shape to those corresponding to the dashed curves in Fig. 6, but their absolute normalization varied. Changes in proton potentials resulted in less than 10% variations in calculated cross sections, while changes in alpha potentials led to $15-20\%$ variations.

The question of the effect of continuous ambiguities in the alpha potential parameters on the energy sharing distributions was also investigated. Calculations with changes in correlated parameters of up to $\pm 20\%$ were carried out. These changes are known to increase the χ^2 for the alpha elastic scattering fits by approximately a factor of 2. The resulting energy sharing distributions had basically the same shape but the overall normalizations varied by up to $\pm 30\%$. Since the (p,pα) reaction is highly surface localized, these variations seem to arise primarily from the changes in the geometrical parameters. Considering the liberal use of variations of a factor of 2 in χ^2, this change must be considered an upper limit estimate of uncertainties due to continuous ambiguities. In addition, since we expect a rather smooth systematic change in the geometrical parameters from nucleus to nucleus, we would estimate the effect on the relative spectroscopic factors for the full range of nuclei studied to be at most about 20%.

In order to investigate the sensitivity to the use of alternative alpha potentials, energy sharing distributions were calculated (see Fig. 7) with the fixed-geometry parameters from each of the two families found by Chang *et al.*[29] for alpha elastic scattering from ^{58}Ni (Table II). Except for the minimum in the ^{48}Ti distribution with the set *B* poten-

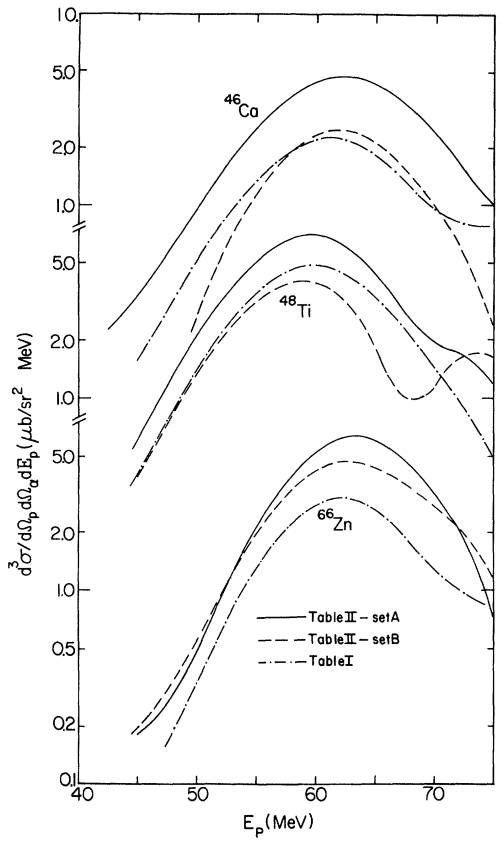

FIG. 7. Comparison of DWIA calculations for ^{40}Ca, ^{48}Ti, and ^{66}Zn using the potentials of Chang *et al.* (Ref. 29) (Table II) with those using the potentials of Table I.

tials, the most significant effect is the change in absolute magnitude of up to 50% for the overall cross section for each target. However, the relative change in cross sections (and therefore the relative spectroscopic factors) for the three targets shown in Fig. 7 is only about 10–25 %, depending on which set is used.

It is difficult to assign an uncertainty in spectroscopic factors arising from the choice of optical model potentials. However, we have examined extreme variations and believe that ±35% is appropriate for uncertainties in the absolute spectroscopic factors arising from the optical model parametrization. Furthermore, this uncertainty will be greatly reduced for relative spectroscopic factors over the full target mass range. Thus, by using systematic optical model potentials we would expect the uncertainties in the relative spectroscopic factors to be no more than ±20% over the full mass range of this work, and that changes in the parameters would result in a monotonic variation of the relative spectroscopic factors.

D. Bound state parametrization

The most significant difficulty in this analysis, as well as the analyses of transfer data, is the treatment of the bound alpha cluster. In terms of the shell model, the wave function for the cluster arises from a complicated overlap integral between the target ground state and the residual nucleus internal wave functions. This overlap generally contains not only the ground state of the alpha particle, but also excited states with different center-of-mass motions of the cluster. One generally assumes that the reaction picks out only the term associated with the ^{4}He ground state configuration. This would appear to be a good approximation, particularly for the highly surface localized (p,pα) reaction. First, the two-body cross section at the light particle vertex associated with changing the configuration from an excited ^{4}He cluster to the ^{4}He ground state (observed in the final state) should be significantly smaller than that associated with p+^{4}He elastic scattering. Second, the cluster c.m. wave function will have a binding energy tail given by the alpha particle separation energy plus the excitation energy in ^{4}He. Since the lowest states in ^{4}He have $E_{ex} \simeq 20$ MeV, the component with an excited cluster will be significantly more tightly bound. Thus, in a strongly surface localized reaction such as (p,pα) (see Sec. IV E) this component will be weakly sampled compared to the ^{4}He ground state component.

Even with this assumption one still has to make a choice of the description of the cluster c.m. wave function. No theoretical work has been done using a shell model basis for this wave function in which account has been taken of the internal energy of the cluster. Treatments such as those used in two-nucleon transfer lead to difficulties in the choice of distribution of the energy among the single particle wave functions.

We have therefore adopted a cluster model approach and calculated the wave function for the interaction of an alpha cluster with the core. As discussed in Sec. IV A, we chose the quantum numbers based on the harmonic oscillator shell model. For the cluster-core interaction we have used two methods. First, we have used a standard Woods-Saxon potential with the well depth chosen to generate a wave function having the correct alpha-particle separation energy. The choice of geometry for this potential has no theoretical guidelines. We have therefore investigated the sensitivity of the calculations to the geometrical parameters, as well as carried out calculations with a geometry identical to that chosen in the (^{6}Li,d) study of Ref. 6. Second, we have calculated the potential by folding an alpha-nucleon interaction into the core density distribution. Such a procedure has been used rather successfully by Buck, Dover, and Vary[30] to reproduce

TABLE II. Parameters for alternative alpha potentials (Ref. 29).

Alpha potential set	V_0 (MeV)	r_0 (fm)	a_0 (fm)	W_0 (MeV)	r_0' (fm)	a_0' (fm)	r_{0_c} (fm)
A	125.65	1.30	0.712	12.28	1.538	0.624	1.40
B	161.78	1.30	0.656	13.71	1.530	0.591	1.40

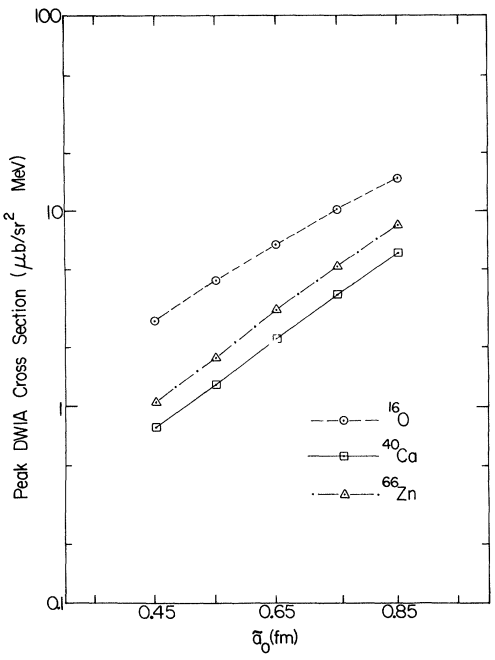

FIG. 8. Peak calculated cross sections for ^{16}O, ^{40}Ca, and ^{66}Zn plotted as a function of the bound state diffuseness parameter, $\tilde{a}_0$.

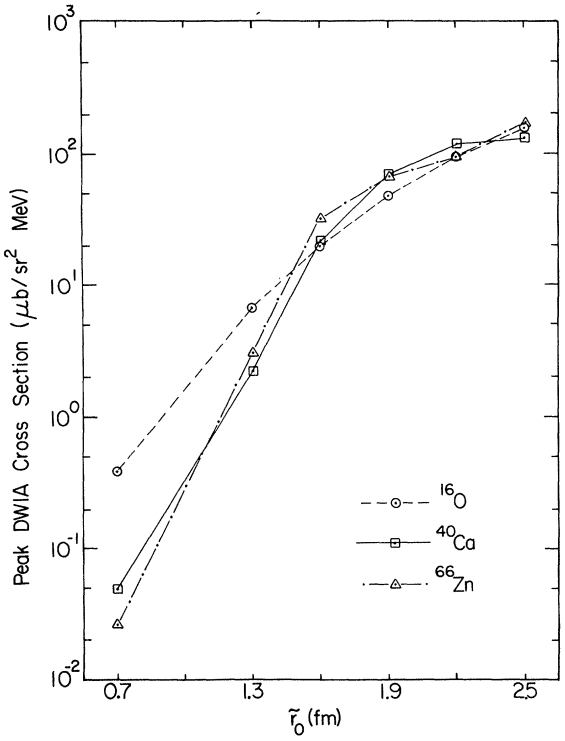

FIG. 9. Peak calculated cross sections for ^{16}O, ^{40}Ca, and ^{66}Zn plotted as a function of the bound state radius parameters, $\tilde{r}_0$.

many of the structure properties of *s-d* shell nuclei.

To investigate the general dependence of the DWIA calculations on the Woods-Saxon bound state geometry, a series of ground state ^{16}O, ^{40}Ca, and ^{66}Zn(p,pα) energy sharing distributions were calculated for various values of the radius parameter $\tilde{r}_0$ and the diffuseness $\tilde{a}_0$. The optical potential parameters in Table I and a constant bound state Coulomb parameter $\tilde{r}_{0_c}=1.3$ fm were utilized. Initially $\tilde{r}_0$ was fixed at 1.3 fm and $\tilde{a}_0$ varied from 0.45 to 0.85 fm in steps of 0.1 fm. The resulting distributions exhibit a common shape which is relatively insensitive to the change in $\tilde{a}_0$. The half width at half maximum decreases rather slowly with an increase in $\tilde{a}_0$, as would be expected from the plane-wave impulse approximation (PWIA). The most significant change is in the absolute magnitude of the overall cross section. Figure 8 shows a plot of the peak cross section as a function of $\tilde{a}_0$. An increase of 25% in $\tilde{a}_0$ raises the theoretical cross section by approximately a factor of 2.5. However, because the trends displayed by the curves in Fig. 8 are all very similar, the relative spectroscopic factors will not be affected by changes in $\tilde{a}_0$ as seriously as the absolute spectroscopic factors.

A similar set of energy sharing distributions was calculated with constant $\tilde{a}_0=0.65$ fm and $\tilde{r}_0$ varying from 0.7 to 2.5 fm in 0.3 fm steps. Figure 9 summarizes the trends observed for the peak cross section. The absolute magnitude of the theoretical cross section is clearly much more sensitive to variations in $\tilde{r}_0$ than it is to changes in $\tilde{a}_0$; a 25% increase in r_0 (near $r_0=1.30$ fm) increases the peak cross section by an order of magnitude. Also contrary to the situation for $\tilde{a}_0$, the target-to-target variance in the trends exhibited by the peak cross section as a function of $\tilde{r}_0$ indicates that the distribution of the relative spectroscopic factors with respect to target mass can be affected by changes in $\tilde{r}_0$. Fortunately, as has been presented in Ref. 13, the widths of the calculated distributions are quite sensitive to the value of $\tilde{r}_0$, especially for the heavier targets. In fact, if we compare these distributions to the measured energy sharing spectra (Fig. 10), we find that as the target mass number increases from 16 to 66 the range of $\tilde{r}_0$ that can be tolerated by the data decreases significantly. Chant[31] has indicated that this bound state selectivity of the (p,pα) reaction may be further enhanced with projectile energies greater than 100 MeV.

Our results suggest that in general $\tilde{r}_0$ must lie roughly within the range from 1.2 to 1.6 fm, with the lower values being more appropriate for the heaviest targets. The statistical errors prevent us from assigning more stringent limits. The use of such values in previous (p,pα) studies has led to absolute spectroscopic factors for 1*p*-shell[14] and light 2*s* 1*d*-shell[15,16] nuclei which agree quite well with those predicted by the shell model. On the other hand, this is in distinct contrast to the situation for (α,2α), where it has been found[31–33] that alpha strengths in agreement with shell model predictions can only be obtained with $\tilde{r}_0=2.5$ fm.

It is clear from this investigation of the sensitivity to the bound state parametrization that it is essential to use a consistent formulation for the cluster-core bound state when comparing structure information extracted from analyses of different reactions for a wide range of targets. Thus, in order to compare our results directly with the systematics obtained by Anantaraman *et al.*,[6] we have

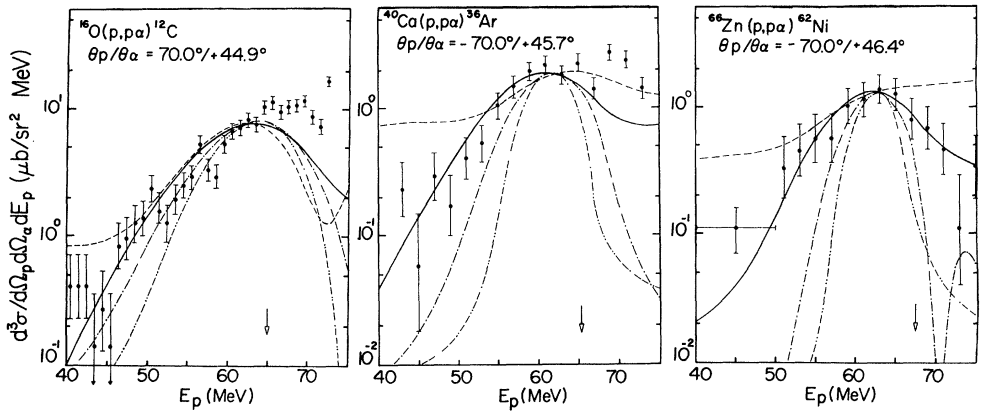

FIG. 10. Comparison of the ground state (p,pα) energy sharing distribution data with DWIA calculations using bound state radius parameters r_0 of 0.7 (— — —), 1.3 (——), 1.9 (— — · — —), and 2.5 (— — ·· — —).

employed their bound state parametrization ($\tilde{r}_0=1.3$ fm and $\tilde{a}_0=0.65$ fm) as our standard in determining alpha spectroscopic factors from the (p,pα) measurements. It should be noted that any systematic change in the radius parameter as a function of mass can drastically change the relative spectroscopic factors extracted from the present data. Thus characterizing the radius of the well by $r_0'(A_c^{1/3}+4^{1/3})$ can lead to significant differences when compared to the radius $r_0A_c^{1/3}$. For example, the use of $r_0'=0.878$, which is equivalent to $r_0=1.3$ for ^{40}Ca, leads to an increase in spectroscopic factors of about a factor of 1.7 for ^{66}Zn and a decrease of about 1.8 for ^{16}O.

An alternative method of generating the cluster-core interaction which possibly has more theoretical justification is that of the folding model. In this model an alpha-nucleon interaction is folded into a nuclear density distribution, thereby providing an alpha-nucleus potential. This technique has been rather successfully applied to calculations of structure properties of 2s-1d shell nuclei,[30] and to the calculation of the real part of the optical potential for alpha-elastic scattering,[34] although in this latter case the imaginary part masks much of the interior of the nucleus.

For the alpha-nucleon interaction we have used the energy dependent potential of Mailandt *et al.*[35] obtained by fitting low energy $p+\alpha$ and $n+\alpha$ elastic scattering. We have taken the parameters appropriate for zero energy. The core densities were taken to be Fermi distributions with the geometrical parameters from Ref. 36 for some nuclei and interpolated values for the few nuclei not included (the neutron and proton density distributions were assumed to be identical). The resultant potential from the folding calculation, along with a Coulomb potential assuming a uniform sphere of charge of radius $1.3A_c^{1/3}$, were put into the bound state code and the folded potential renormalized until the alpha particle separation energy was reproduced. The resultant wave function was then used in the DWIA calculation.

One disquieting feature of this calculation was the large renormalization of the folded potential required. The folded potentials were approximately a factor of 5 deeper than that required to bind the alpha cluster in the appropriate oscillator quantum state. This casts doubt on this simple model, and perhaps many effects such as the Pauli principle need to be included. However, if one takes the attitude that those effects are largely included by the renormalization process, the calculation provides us with a well-defined method of putting the mass dependence into the geometry of the potential. This is as opposed to the rather arbitrary method of using a Woods-Saxon potential with a radius parameter of $r_0A_c^{1/3}$ or $r_0'(A_c^{1/3}+4^{1/3})$. It should also be noted that the resultant potentials are consistent with those obtained by Buck *et al.*[30]

In Fig. 11 the potentials and wave functions for ^{16}O, ^{40}Ca, and ^{66}Zn obtained from the folding calculations (dashed lines) are compared with those of the Woods-Saxon (WS) well (solid lines). The former has a smaller radius, larger depth and diffuseness, and as a result the wave function is more compressed. The difference is smaller for the light nuclei and larger for the heavier nuclei.

E. Radial localization of the (p,pα) reaction

Before examining the spectroscopic factors extracted from the DWIA analysis, we examine the sensitivity of the (p,pα) reaction to various radial regions of the nucleus. Figure 12 displays histograms of the contributions to the DWIA cross section as a function of radius for the (p,pα) ground state transition zero-recoil momentum point. The quantity $\Delta\sigma$ represents the change in cross section as a function of cutoff radius; i.e.,

$$\Delta\sigma=\sigma(R)-\sigma(R+\Delta)\ ,$$

where $\sigma(x)$ is the differential cross section calculated with a cutoff radius of x. The smooth curves depict the radial dependence of the cluster-core bound state radial wave functions for the Woods-Saxon potential. The dashed curves represent a Fermi charge distribution fitted to electron scattering.[36]

It is evident that for low recoil momenta the (p,pα) reaction is strongly surface localized, the major contributions coming from the few percent nuclear density region. We also note in all cases a rather strong destructive interference contribution just past the last node in the radial

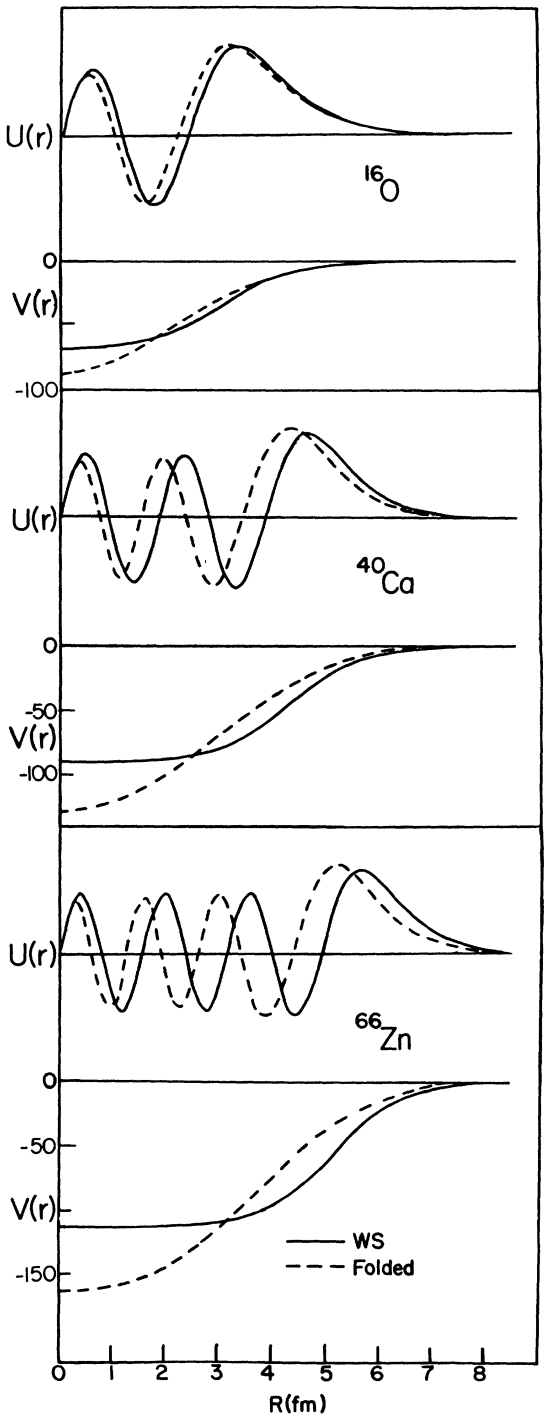

FIG. 11. Comparison of potentials and wave functions for ^{16}O, ^{40}Ca, and ^{66}Zn bound alpha clusters obtained from the folding model with those of the WS potential.

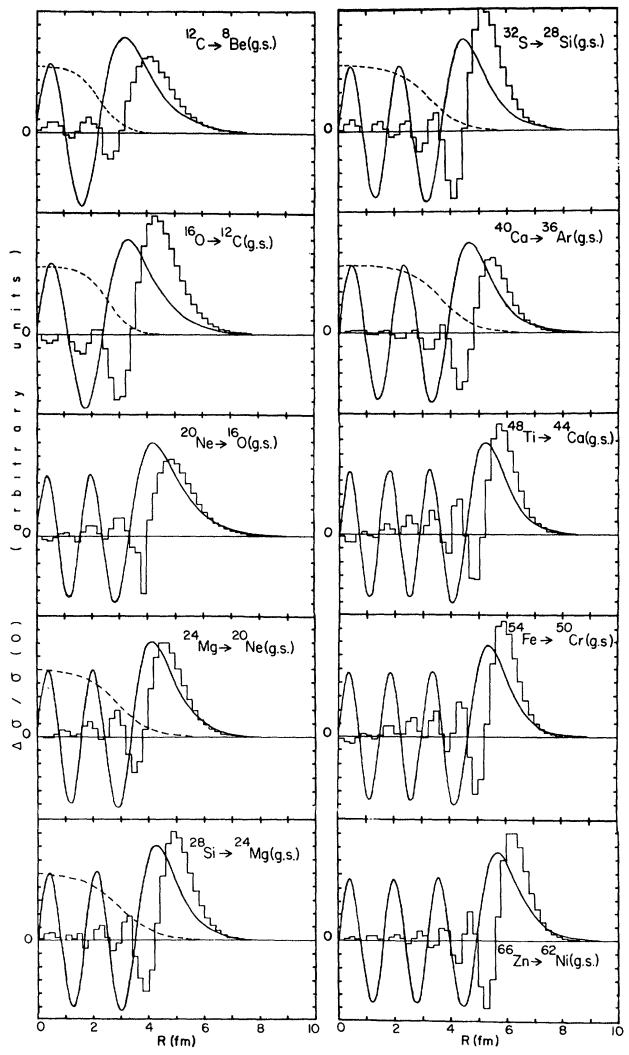

FIG. 12. Radial distributions of the DWIA cross sections for the (p,pα) reaction at 100 MeV (histograms). The solid curves represent the bound alpha cluster wave functions. Also shown are the nuclear charge density distributions where available (dashed curve).

wave function. Due to this interference and to the effects of absorption the (p,pα) reaction at 100 MeV is predominantly sensitive to the asymptotic properties of the bound state, and cannot be used to probe the interior of the nucleus. This surface localization should enhance the accuracy of the factorization approximation, since the contributions come from regions where the scattered particles have almost their asymptotic momenta, assuming, of course, that finite range effects produce no significant changes in the radial contributions.

F. Ground state spectroscopic factors

Using the distorting potentials given in Table I and the standard Woods-Saxon bound state parameters, ground state energy sharing spectra were calculated for all targets. These are shown as solid lines in Fig. 3, normalized to the data. In normalizing the calculations particular attention was paid to avoiding processes not included in the DWIA, such as the sequential process. Thus, the higher proton energy region, where sequential processes are expected, were to a large extent ignored.

With the exception of ^{28}Si, the shapes of the energy sharing distributions are well reproduced. For ^{28}Si the shape of the experimental spectrum suggests the presence

TABLE III. Absolute alpha spectroscopic factors for ground state transitions.

(p,pα) transition	S_α^{exp} (WS)	S_α^{exp} (folded)	S_α^{SM}[a]	$S_\alpha^{SU(3)}$[b]	$\frac{S_\alpha^{exp}}{S_\alpha^{SM}}$	$\frac{S_\alpha^{exp}}{S_\alpha^{SU(3)}}$
$^{12}C\rightarrow{}^{8}Be$	0.72±0.07	0.65	0.56	0.68	1.3	1.1
$^{16}O\rightarrow{}^{12}C$	1.15±0.1[c]	1.66	0.23	0.30	5.0	3.8
$^{20}Ne\rightarrow{}^{16}O$	0.54±0.08	0.64	0.18	0.23	3.0	2.4
$^{24}Mg\rightarrow{}^{20}Ne$	0.42±0.05	0.51	1.11	0.081	3.8	5.2
$^{28}Si\rightarrow{}^{24}Mg$	0.20±0.04 (0.50±0.07)	0.40	0.076	0.094	2.6 (6.6)	2.1 (5.3)
$^{32}S\rightarrow{}^{28}Si$	0.55±0.07	1.50	0.090		6.1	
$^{40}Ca\rightarrow{}^{36}Ar$	0.86±0.09	3.98	0.043		20.0	
$^{48}Ti\rightarrow{}^{44}Ca$	0.22±0.04	1.06				
$^{54}Fe\rightarrow{}^{50}Cr$	0.16±0.03	0.84				
$^{66}Zr\rightarrow{}^{62}Ni$	0.42±0.05	6.84				

[a]Reference 38.
[b]Reference 39.
[c]Both the O_2 gas and the SiO_2 solid targets gave identical values for ^{16}O.

of two competing processes leading to a relatively narrow structure centered about $E_p \approx 65$ MeV (possibly due to sequential processes) superimposed on a much broader underlying distribution which is more characteristic of knockout reactions. Thus, the calculations were normalized to the latter.

Also shown in Fig. 3, as dashed curves, are the results of the folding model calculations again normalized to the data. One observes that the shapes are nearly identical to those obtained with the Woods-Saxon potential. This is presumably due to the similarity of the rms radii of the wave functions.

The absolute ground state spectroscopic factors thereby extracted are summarized in Table III. These have already been presented in Ref. 12 and are reviewed here. Also included are available theoretical shell model estimates by Kurath[37] and by Chung *et al.*,[38] as well as results from Draayer's SU(3) calculations.[39] To allow some measure of comparison with the 1*p*-shell study by Roos *et al.*,[14] we used their data and the ingredients of our analysis to extract a spectroscopic factor for $^{12}C(p,p\alpha)^{8}Be(g.s.)$ at 100 MeV with $\theta_p/\theta_\alpha = -75.0°/+43.1°$. In the case of ^{28}Si, the spectroscopic factor obtained by normalizing to the peak at ~65 MeV is enclosed in parentheses. The error bounds stated for the experimental values only include contributions from the experimental uncertainties in the measured cross sections. The typical error is in the range from ~10% to 15%, although for ^{28}Si even a value as large as ±20% may not be liberal enough. Also, it might be argued that an additional ±10% uncertainty should be folded into each of these limits to account for the potential errors in our estimates for the on-shell p-α cross sections.

The resultant spectroscopic factors show a large difference between the Woods-Saxon potential and the folded potential. In the low mass region the two calculations produce similar results. However, for the heaviest mass the folded potential leads to a spectroscopic factor 16 times as large. Thus, the two calculations lead to rather different mass dependence. This result reemphasizes the need for theoretical guidance in the treatment of the cluster wave function.

Before discussing the absolute spectroscopic factors further, let us consider the comparison to other experimental results. It is perhaps natural to attempt a direct comparison of the absolute spectroscopic factors measured in this experiment with those obtained from other alpha-removal investigations at comparable energies; but, differences in the ingredients of the respective theoretical analyses, particularly the bound state treatment, can lead to considerable complications. Recalling the restricted nature of our analysis, we instead concentrate on a survey of the mass dependence of the *relative* ground state spectroscopic factors first observed in the (^{6}Li,d) studies.[6] A plot of these results is shown in Fig. 1, along with our present results using the same Woods-Saxon bound state geometry. The data points from each reaction have been normalized such that

$$S^{rel}[^{20}Ne(g.s.) \rightleftarrows {}^{16}O(g.s.)+\alpha] = 1 \ .$$

In addition, only the points corresponding to even-even (p,pα) targets have been taken from Ref. 6, since it has lately become evident that the alpha transfer process is sensitive to neutron and proton pairing correlations and hence exhibits rather dissimilar features for odd-*A* targets as compared to even-*A* targets.[40]

The agreement between the two trends displayed here is striking, especially in view of recent indications[11,12] that variations in only the optical potentials can lead to drastically different systematics for $A_T \gtrsim 50$ in the alpha transfer analyses (see Fig. 1). Given the substantial differences between the (p,pα) and the (^{6}Li,d) reaction dynamics and the consistency of our analysis, we conclude that this oscillatory behavior of the values of S^{rel} is indicative of a nuclear *structure* effect, as long as the Woods-Saxon bound state treatment is applicable. Since the present (p,pα) results are relatively insensitive to optical model treatments (at the level of 30%), we believe that the reanalysis of the (^{6}Li,d) data with modified optical potentials[11,12] in order to reproduce shell model trends, may be

an incorrect and misleading analysis. Rather that changes in the mass dependence of the S_α will have to come as a result of a more sophisticated treatment of the bound cluster.

The absolute alpha spectroscopic factors determined using the Woods-Saxon bound state analysis are consistently larger than the corresponding shell model predictions. Still, at the lower end of the $2s\,1d$ shell, where one might expect *sd*-shell-model calculations to be most reliable, the ratio of the experimental to shell model values is roughly constant at 3. Such a discrepancy can readily be removed through an increase in the bound state radius parameter of $\lesssim 12\%$, a modification which is well within the restrictions imposed by the energy sharing data. Also, the somewhat larger disagreement between experiment and shell model for the heavier $2s\,1d$-shell nuclei may reflect the restricted basis used in the theoretical calculations rather than any real physical effects. Furthermore, it may be only due to the restricted shell model basis that for both the $1p$ and $2s\,1d$ shells the largest discrepancies between experiment and theory occur at the doubly magic $4n$ nuclei which close those shells. The situation with respect to the SU(3) spectroscopic factors is qualitatively the same as that for the shell model predictions.

For the $1f\,2p$-shell targets, only a very limited number of calculations have been reported. Perhaps the most complete to date are those by Bennett *et al.*,[41] which employed the full $(1f_{5/2},2p_{3/2},2p_{1/2})^n$ shell model space. However, even allowing for representation mixing they predict a

$$^{66}\mathrm{Zn(g.s.)} \rightleftarrows {}^{62}\mathrm{Ni(g.s.)}+\alpha$$

absolute spectroscopic factor of only ~ 0.02, which is smaller than our measured value by a factor of 20. The results of Sec. IV D suggest that no reasonable variation of the bound state geometry can reduce the experimental value by this amount. Thus, important configurations are still likely to be missing from theoretical basis space; and a full understanding of the measured *fp*-shell spectroscopic factors awaits a more extensive set of calculations. In this regard it is worth noting that for the heaviest mass nuclei theoretical calculations predict α-decay widths which differ by several orders of magnitude from experiment in the same direction as the present spectroscopic factors. With respect to the folding model treatment we obtain even larger spectroscopic factors, with the magnitude increasing greatly for the heavier elements. Again, assuming the appropriateness of the folding model treatment, these results suggest significantly stronger configuration mixing than that contained in present shell model calculations. The differences obtained from the two types of analyses emphasize the necessity for a proper treatment of the alpha cluster wave function.

G. Spectroscopic factors for excited state transitions

Data were also obtained for eight excited states. While of poorer statistical accuracy, the associated spectra still permit the extraction of spectroscopic strengths within a factor of 2. DWIA energy sharing distributions were calculated for these states with the standard Woods-Saxon bound state geometry and optical potentials in Table I; no parameter variations were made to obtain improved fits to the experimental data.

The resulting fits are shown by the solid curves in Fig. 4. Except for ^{40}Ca and ^{66}Zn, they are rather disappointing. Perhaps variations in the parameters would lead to some improvement, but it is unlikely that this would produce any large changes in the magnitudes of the theoretical cross sections relative to the ground states. The absolute spectroscopic factors corresponding to these normalizations are presented in Table IV, along with their ratios to the ground states to facilitate comparison with alpha transfer data. The errors represent variations in the normalizations which do not lead to significant deterioration in the fits.

The extracted spectroscopic factors are all generally higher than theoretical predictions and available measurements from alpha transfer reactions, except for ^{24}Mg(p,pα)^{20}Ne(2^+) and ^{40}Ca(p,pα)^{36}Ar(2^+) which show good agreement with the 70 MeV (^{3}He,^{7}Be) and 35 MeV (d,^{6}Li) results, respectively. These large spectroscopic factors are somewhat suggestive of contributions from multistep processes. However, before such a claim can be substantiated, a more detailed DWIA analysis is in order, including variation of the optical potentials and bound state parameters. Furthermore, data with much better statistics would be most useful. With respect to multistep processes we note that the ground state peak cross sections, where the DWIA normalization is made, are at least one order of magnitude larger than the excited state cross sections. Therefore, we expect little sensitivity to these higher order processes, if they are present.

V. DISCUSSIONS AND CONCLUSIONS

The (p,pα) experimental data for nine targets were obtained with a binding energy resolution sufficient to provide clean separation between the ground and low-lying excited states of all the residual nuclei. Excited state transition data were also obtained for a number of nuclei.

The data were analyzed in a consistent manner, especially with respect to the choice of distorting potentials and bound state wave functions, and detailed studies on the sensitivities of the results to their parametrization were carried out, both with regards to an absolute accuracy of the spectroscopic factors and to the features of any systematic trend they might exhibit on a relative basis. Distorting potentials seem to affect extraction of only the absolute spectroscopic factors but not relative spectroscopic factors. Therefore, erroneous choices of distorting parameters could lead to fairly large uncertainties in the absolute spectroscopic factors, but for target-to-target comparison the relative spectroscopic factor would be far more reliable, as long as a given family of potentials is maintained for all the analyses.

The DWIA cross sections show an extreme and quite strong target-dependent sensitivity both in magnitude and shape to variations in the bound state geometry, particularly the radius parameter. Comparisons with the measured energy sharing spectra restrict the radius parameter to a range of values which decreases significantly as the

TABLE IV. Comparison of excited-state spectroscopic factors.

Transition	101.5 MeV (p,pα) absolute	101.5 MeV (p,pα) relative	Theory: 1p shell model[a] absolute	Theory: 1p shell model[a] relative	157 MeV (p,pα)[f] relative	80 MeV (d,^{6}Li)[b] relative	54 MeV (d,^{6}Li)[g] relative	70 MeV (α,^{8}Be)[c] relative	35 MeV (d,^{6}Li)[h] relative	70 MeV (^{3}He,^{7}Be)[d] relative
$^{16}O \rightarrow {}^{12}C$										
[0$^+$(g.s.)]	1.15±0.1	1	0.23	1		1		1		1
[2$^+$(4.4)]	15.0 ±7	13.0±6	1.30	5.65		4.84		4.28		2.03
[4$^+$(14.1)]	56±20	49±18	2.38	10.3		7.71		5.60		
$^{24}Mg \rightarrow {}^{20}Ne$			SU(3)[e] absolute	SU(3)[e] relative						
[0$^+$(g.s.)]	0.42±0.05	1	0.081	1	1		1	1	1	1
[2$^+$(1.6)]	0.90±0.5	2.1±1.2	0.012	0.14	0.9±0.5		0.43	0.90		2.0
$^{32}S \rightarrow {}^{28}Si$										
[0$^+$(g.s.)]	0.55±0.07	1								
[2$^+$(1.8)]	3.5 ±0.7	6.4±1.3								
$^{40}Ca \rightarrow {}^{36}Ar$			SU(3)[e] 2s 1d shell model[i] relative	SU(3)[e] 2s 1d shell model[i] relative	157 MeV (p,pα)[f] relative	80 MeV (d,^{6}Li)[j] relative	54 MeV (d,^{6}Li)[k] relative	70 MeV (α,^{8}Be)[c] relative	35 MeV (d,^{6}Li)[l] relative	70 MeV (^{3}He,^{7}Be)[d] relative
[0$^+$(g.s.)]	0.86±0.09	1	1	1	1	1	1	1	1	1
[2$^+$(2.0)]	5.9 ±0.8	6.9±1.2	5.0	6.25	1.8±1	2.3–2.9	0.97	5.60		1.0
[4$^+$(4.4)]	26.0±9	30 ±11		10.4		3.8–5.4	1.25			
$^{54}Fe \rightarrow {}^{50}Cr$										
[0$^+$(g.s.)]	0.16±0.03	1								
[2$^+$(0.8)]	0.66±0.3	4.1±2								
$^{66}Zn \rightarrow {}^{62}Ni$										
[0$^+$(g.s.)]	0.42±0.05	1								
[2$^+$(1.2)]	0.78±0.3	1.9±0.8								

[a]Reference 37.
[b]Reference 42.
[c]Reference 43.
[d]Reference 7.
[e]References 16 and 39.
[f]Reference 16.
[g]Reference 44.
[h]Reference 45.
[i]Reference 38.
[j]Reference 46.
[k]Reference 47.
[l]Reference 48.

target mass increases. It has been pointed out that this $\tilde{r}_0$ selectivity of the (p,pα) reaction may be further enhanced with increasing projectile energy. This, coupled with the fact that alpha potentials become less ambiguous at higher energies, seems to suggest that more reliable spectroscopic factors could be extracted by performing (p,pα) reactions at higher energies.

In spite of the associated uncertainties, it is found that with consistent analyses employing a common bound state formulation, the alpha knockout and transfer reactions provide remarkably similar behaviors for the mass dependence of the relative alpha spectroscopic factors of nuclei in the $2s\,1d$ and $1f\,2p$ shells. Given the major differences between these two approaches in terms of reaction dynamics (quasifree scattering at fairly high energy versus quasi-alpha "capture" at rather low effective energy), reaction kinematics (small versus large momentum transfers), and phenomenological requirements (optical potentials for single particles or tightly-bound clusters versus those for weakly bound, very strongly absorbed composite projectiles), it would be truly surprising if the extent of the agreement between the two trends shown in Fig. 1 was purely coincidental and not indicative of a real nuclear-structure effect.

The use of a folded alpha-core bound-state potential leads to spectroscopic factors which increase greatly with increasing mass. Whether this model is more appropriate than the use of a constant radius parameter is uncertain. However, the two treatments clearly point to the great need for theoretical guidance in the treatment of the alpha-cluster wave function. We believe that the (p,pα) reaction provides the best tool for extracting ground state absolute spectroscopic information for nuclei, and these data can provide that information when the theoretical advances discussed have been made.

The situation for the excited states is markedly different. In addition to the data having large statistical uncertainties, DWIA calculations with the same distorting potentials and bound state geometry as those used for the ground state transitions poorly reproduce the excited-state energy sharing distributions. Most of the extracted spectroscopic factors seem to be unreasonably large. It is therefore desirable to have better quality data to test the theoretical predictions.

ACKNOWLEDGMENTS

The authors are grateful to the University of Maryland Computer Science Center for its generous allocation of computer time. This work was supported in part by the National Science Foundation.

*Present address: P Division, Los Alamos Scientific Laboratory, Los Alamos, NM 87545.

†Present address: University of Michigan-Dearborn, 4901 Evergreen Road, Dearborn, MI 48128.

‡Present address: Department of Physics, Towson State University, Baltimore, MD 21204.

[1]G. Gamow, Z. Phys. 51, 204 (1928).

[2]W. von Oertzen, in *Proceedings of the Second International Conference on Clustering Phenomena in Nuclei, College Park, 1975,* edited by D. A. Goldberg, J. B. Marion, and S. J. Wallace (National Technical Information Service, Springfield, Virginia, 1975), p. 367.

[3]M.-C. Lemaire, Phys. Rep. 7, 279 (1973).

[4]H. H. Gutbrod, H. Yoshida, and R. Bock, Nucl. Phys. A165, 240 (1971).

[5]F. D. Becchetti, L. T. Chua, J. Jänecke, and A. M. Vander Molen, Phys. Rev. Lett. 34, 225 (1975).

[6]N. Anantaraman *et al.,* Phys. Rev. Lett. 35, 1131 (1975).

[7]W. F. Steele, P. A. Smith, J. E. Finck, and G. M. Crawley, Nucl. Phys. A266, 424 (1976).

[8]G. Audi, C. Détraz, M. Langevin, and F. Pougheon, Nucl. Phys. A237, 300 (1975).

[9]P. G. Roos and N. S. Chant, in *Proceedings of the Second International Conference on Clustering Phenomena in Nuclei, College Park, 1975,* edited by D. A. Goldberg, J. B. Marion, and S. J. Wallace, (National Technical Information Service, Springfield, Virginia, 1975), p. 242.

[10]V. V. Balyshov, in *Clustering Aspects of Nuclear Structure and Nuclear Reactions, Winnipeg, 1978,* Proceedings of the Third International Conference on Clustering Aspects of Nuclear Structure and Nuclear Reactions, AIP Conf. Proc. No. 47, edited by W. T. H. Van Oers, J. P. Svernne, J. S. C. McKee, and W. R. Falk (AIP, New York, 1978), p. 252.

[11]H. W. Fulbright *et al.,* Nucl. Phys. A284, 329 (1977).

[12]N. Anantaraman, H. W. Fulbright, and P. M. Stwertka, Phys. Rev. C 22, 501 (1980).

[13]T. A. Carey, P. G. Roos, N. S. Chant, A. Nadasen, and H. L. Chen, Phys. Rev. C 23, 576 (1981).

[14]P. G. Roos *et al.,* Phys. Rev. C 15, 69 (1977).

[15]R. I. Steinberg *et al.,* in *Proceedings of the Second International Conference on Clustering Phenomena in Nuclei, College Park, 1975,* edited by D. A. Goldberg, J. B. Marion, and S. J. Wallace (National Technical Information Service, Springfield, Virginia, 1975), p. 315.

[16]D. Bachelier *et al.,* Nucl. Phys. A268, 488 (1976).

[17]N. S. Chant and P. G. Roos, Phys. Rev. C 15, 57 (1977).

[18]S. M. Bunch, H. H. Forster, and C. C. Kim, Nucl. Phys. 53, 241 (1964).

[19]M. K. Brussel and J. H. Williams, Phys. Rev. 106, 286 (1957).

[20]B. W. Davies *et al.,* Nucl. Phys. A97, 241 (1967).

[21]S. Hayakawa *et al.,* J. Phys. Soc. Jpn. 19, 2004 (1964).

[22]L. G. Votta, P. G. Roos, N. S. Chant, and R. Woody, III, Phys. Rev. C 10, 520 (1974).

[23]N. P. Goldstein, A. Held, and D. G. Stairs, Can. J. Phys. 48, 2629 (1970).

[24]A. M. Cormack, J. N. Palmieri, N. F. Ramsey, and Richard Wilson, Phys. Rev. 115, 599 (1959).

[25]A. Nadasen, Ph.D. thesis, Indiana University, 1977; A. Nadasen *et al.,* Phys. Rev. C 23, 1023 (1981).

[26]D. A. Goldberg, S. M. Smith, and G. F. Burdzik, Phys. Rev. C 10, 1362 (1974), and references therein.

[27]C. M. Perey and F. G. Perey, At. Data Nucl. Data Tables 17, 1 (1976).

[28]L. W. Put and A. M. J. Paans, Nucl. Phys. A291, 93 (1977).

[29]H. H. Chang *et al.,* Nucl. Phys. A270, 413 (1976).

[30]B. Buck, C. B. Dover, and J. P. Vary, Phys. Rev. C 11, 1803 (1975).

[31]N. S. Chant, in *Clustering Aspects of Nuclear Structure and*

Nuclear Reactions, Winnipeg, 1978, Proceedings of the Third International Conference on Clustering Aspects of Nuclear Structure and Nuclear Reactions, AIP Conf. Proc. No. 47, edited by W. T. H. Van Oers, J. P. Svernne, J. S. C. McKee, and W. R. Falk (AIP, New York, 1978), p. 415.

[32]C. W. Wang *et al.,* Phys. Rev. C 21, 1705 (1980).

[33]N. S. Chant, P. G. Roos, and C. W. Wang, Phys. Rev. C 17, 8 (1978).

[34]D. F. Jackson and V. K. Kembhavi, Phys. Rev. 178, 1626 (1969); P. P. Singh, P. Schwandt, and G. C. Yang, Phys. Lett. 59B, 113 (1975).

[35]P. Mailandt, J. S. Lilley, and G. W. Greenlees, Phys. Rev. C 8, 2189 (1973).

[36]L. R. B. Elton, *Nuclear Sizes* (Oxford University, London, 1961), p. 31.

[37]D. Kurath, Phys. Rev. C 7, 1390 (1973).

[38]W. Chung, J. van Hienen, B. H. Wildenthal, and C. L. Bennett, Phys. Lett. 79B, 381 (1978).

[39]J. P. Draayer, Nucl. Phys. A237, 157 (1975); K. T. Hecht and D. Braunschweig, *ibid.* A244, 365 (1975).

[40]D. L. Hanson *et al.,* in *Clustering Aspects of Nuclear Structure and Nuclear Reactions, Winnipeg, 1978,* Proceedings of the Third International Conference on Clustering Aspects of Nuclear Structure and Nuclear Reactions, AIP Conf. Proc. No. 47, edited by W. T. H. Van Oers, J. P. Svernne, J. S. C. McKee, and W. R. Falk (AIP, New York, 1978), p. 716; M. A. Eswaran and H. E. Gove, Phys. Rev. C 18, 1528 (1978).

[41]C. L. Bennett *et al.,* Phys. Rev. C 19, 1099 (1979).

[42]M. G. Betigeri *et al.,* in *Clustering Aspects of Nuclear Structure and Nuclear Reactions, Winnipeg, 1978,* Proceedings of the Third International Conference on Clustering Aspects of Nuclear Structure and Nuclear Reactions, AIP Conf. Proc. No. 47, edited by W. T. H. Van Oers, J. P. Svernne, J. S. C. McKee, and W. R. Falk (AIP, New York, 1978), p. 706.

[43]G. J. Wozniak, D. P. Stahel, Joseph Cerny, and N. A. Jelly, Phys. Rev. C 14, 815 (1976).

[44]K. Takimoto *et al.,* in *Clustering Aspects of Nuclear Structure and Nuclear Reactions, Winnipeg, 1978,* Proceedings of the Third International Conference on Clustering Aspects of Nuclear Structure and Nuclear Reactions, AIP Conf. Proc. No. 47, edited by W. T. H. Van Oers, J. P. Svernne, J. S. C. McKee, and W. R. Falk (AIP, New York, 1978), p. 710.

[45]J. D. Cossairt *et al.,* Nucl. Phys. A261, 373 (1976).

[46]W. Oelert *et al.,* Phys. Rev. C 20, 459 (1979).

[47]T. Yamaya *et al.,* in *Clustering Aspects of Nuclear Structure and Nuclear Reactions, Winnipeg, 1978,* Proceedings of the Third International Conference on Clustering Aspects of Nuclear Structure and Nuclear Reactions, AIP Conf. Proc. No. 47, edited by W. T. H. Van Oers, J. P. Svernne, J. S. C. McKee, and W. R. Falk (AIP, New York, 1978), p. 712.

[48]A. Vander Molen, J. Janecke, and F. D. Becchetti, in *Proceedings of the Second International Conference on Clustering Phenomena in Nuclei, College Park, 1975,* edited by D. A. Goldberg, J. B. Marion, and S. J. Wallace (National Technical Information Service, Springfield, Virginia, 1975), p. 413.